Utility of Lyapunov Orbit Manifold Trajectories within the Saturn-Titan System

Miles Puchner[1], Eric Foss[2], and Dave Boisie Laygo[3]

[1]UC San Diego, Department of Mechanical and Aerospace Engineering

13 June 2024

For space mission operations, orbit determination (OD) is a crucial aspect for predicting orbital trajectories and transfers of spacecraft. To describe the motion of these objects in space under the influence of gravitational and other perturbing forces, mathematical models are derived based on Newton's governing laws of gravitation and motion. In this report, we explore one of these simplified models, the Circular Restricted Three-Body Problem (CR3BP), that describes the motion of a small object under the gravitational influence of two larger primary bodies that are in a circular orbit about their barycenter. We apply this model to a proposed scientific mission to Saturn's largest moon Titan. By leveraging the stable and unstable manifold dynamics associated with the Lagrange points of the Saturn-Titan system, we derive a series of optimal low-energy transfer trajectories for landing a spacecraft on the surface of Titan.

1 Introduction

Based on the recent discoveries by NASA's Cassini Spacecraft, Saturn's largest moon, Titan, has captured significant scientific attention as a potentially life-harboring and hospitable world within our solar system. With both a dense nitrogen-based atmosphere and an earth-like liquid cycle on its surface, Titan has been speculated to have a high likelihood of hosting extraterrestrial life [1]. The more favorable environmental conditions in comparison to other rocky worlds, also suggests the potential for human habitation with minimal technological support required to sustain life [2]. With the conclusion of the Cassini-Huygens mission in 2017, embarking on a new expedition to the richly organic moon would prove valuable for advancing the search for extraterrestrial life in our solar system. Specifically, sending a spacecraft equipped with a rover or drone payload to directly explore the surface of Titan would serve as the next step in investigating the life-harboring potential of this primordial Earth-like world [3].

Due to the significant distance between the Saturn system and Earth, combined with the high-risk payload of the spacecraft, incorporating low-cost and optimal trajectories are essential to minimizing the mission's overall cost. In predicting these orbital trajectories within the Saturn-Titan system, we simplify the dynamics to a CR3BP model given the relatively small mass of the spacecraft relative to the larger mass of Saturn and Titan. The overall mass ratio of the system ($\mu = 0.000237$) is also relatively small, making it a fairly tractable and solvable orbital system. With the CR3BP, the existence and globalization of stable and unstable manifolds about the Lagrange points of the system reveals a set of cylindrical tubes or "transport networks" that can be exploited to design optimal low-cost trajectories for interplanetary transfer [3] [4].

The objective of this paper is to derive the most optimal transfer trajectories from local Lyapunov orbits around the Saturn-Titan system Lagrange points, to an ideal orbital trajectory for landing on Titan's surface, through analysis of the orbital system using the CR3BP model.

2 Problem Statement

2.1 The CR3BP Equations of Motion in the Synodic Frame

The CR3BP aims to determine the equations of motion for a third body that feels the gravitational effects from two, much larger primaries. Therefore, the assumption that the third smaller body does not affect the primaries is made (i.e. $\mu_3 << \mu_1 \approx \mu_2$). In general, we can state the force potential on the third body relative to the primaries' barycenter as

$$U = \sum_{i=1}^{2} \frac{Gm_i}{r_{i,3}} = \frac{\mu_1}{|\boldsymbol{r} - \boldsymbol{r}_1|} + \frac{\mu_2}{|\boldsymbol{r} - \boldsymbol{r}_2|} \tag{2.1.1}$$

where $G = 6.6742x10^{-11}\ Nm^2kg^{-2}$ is the universal gravitational constant, m_i is the mass of primary i, and $r_{i,3} = |\boldsymbol{r}_{i,3}| = |\boldsymbol{r}_3 - \boldsymbol{r}_i|$ is the distance the third body is from primary i. We also note that $\boldsymbol{r}_3 = x\hat{\boldsymbol{x}} + y\hat{\boldsymbol{y}} + z\hat{\boldsymbol{z}}$ and $\boldsymbol{r}_i = x_i\hat{\boldsymbol{x}} + y_i\hat{\boldsymbol{y}} + z_i\hat{\boldsymbol{z}}$ are the distances the third body and primary i are from the barycenter respectively.

A useful form of the equations of motion is often found by using the synodic frame. In this frame, we define the primaries to lay on the x-axis with the origin corresponding to their barycenter. We then let the frame rotate at

$$\boldsymbol{\omega} = \sqrt{\frac{G(m_1 + m_2)}{R(t)^3}}\,\hat{\boldsymbol{z}}, \quad \boldsymbol{R}(t) = \boldsymbol{r_2} - \boldsymbol{r_1}, \tag{2.1.2}$$

where ω is the rate at which the primaries rotate about their barycenter and $\boldsymbol{R}$ is the distance between the primaries. From the conservation of linear momentum, we also know that

$$m_1\boldsymbol{r_1} + m_2\boldsymbol{r_2} = \boldsymbol{0} \tag{2.1.3}$$

which allows for the distance the primaries are from their barycenter to be cast in terms of their masses and the total distance between them. Specifically,

$$\boldsymbol{r_1} = -\frac{m_2}{m_1 + m_2}\boldsymbol{R}(t), \quad \boldsymbol{r_2} = \frac{m_1}{m_1 + m_2}\boldsymbol{R}(t). \tag{2.1.4}$$

We then introduce a mass ratio μ for convenience which allows the above equations to follow as

$$\boldsymbol{r_1} = -\mu\boldsymbol{R}(t), \quad \boldsymbol{r_2} = (1 - \mu)\boldsymbol{R}(t), \quad with \quad \mu = \frac{m_2}{m_1 + m_2}. \tag{2.1.5}$$

This new simplification allows the force potential U to be written as

$$U = \frac{\mu_1}{|\boldsymbol{r} + \mu\boldsymbol{R}(t)|} + \frac{\mu_2}{|\boldsymbol{r} - (1 - \mu)\boldsymbol{R}(t)|}. \tag{2.1.6}$$

It is here that we note the significance of a circular orbit. In a general orbit, the distance between the primaries $\boldsymbol{R}(t)$ is a function of time. For instance, if the primaries orbit in an ellipse, then the distance between them will oscillate between a maximum and minimum value as they travel between the apses. As a result, the distance between them will depend on their respective positions within the orbit. However, if the orbit is circular, then the primaries will always be at a constant distance from each other. This removes the time dependence in the total distance ($\boldsymbol{R}(t) = \boldsymbol{R}$), simplifying the problem greatly.

We will return to the significance of this time dependence when developing the Jacobi Integral later. For now, we will simply cast this new potential into a rotating frame using the transport theorem. It should be noted that up until this point, every variable has been relative to an inertial barycentric frame. As such, we have left out any subscripts representative of this frame for conciseness. In general, the transport theorem follows as

$$\boldsymbol{r_I} = \boldsymbol{r_R}, \quad \dot{\boldsymbol{r_I}} = \dot{\boldsymbol{r_R}} + \boldsymbol{\omega} \times \boldsymbol{r_R}, \tag{2.1.7}$$

where the subscripts $'I'$ and $'R'$ represent inertial and rotating frames respectively. The force potential U has the same form in the rotating frame as in the inertial, however, if we apply the transport theorem to the kinetic energy we obtain

$$T = \frac{1}{2}\dot{\boldsymbol{r}}_{\boldsymbol{I}} \cdot \dot{\boldsymbol{r}}_{\boldsymbol{I}} = \frac{1}{2}\dot{\boldsymbol{r}}_{\boldsymbol{R}} \cdot \dot{\boldsymbol{r}}_{\boldsymbol{R}} + \dot{\boldsymbol{r}}_{\boldsymbol{R}} \cdot \tilde{\boldsymbol{\omega}} \cdot \boldsymbol{r}_{\boldsymbol{R}} + \frac{1}{2}\omega^2(x^2 + y^2) \tag{2.1.8}$$

where we have introduced ~ over a variable to represent a cross-product in dyadic notation.

To continue the derivation, we employ the use of Lagrangian dynamics in which the equations of motion can be found by defining the Lagrangian L in the rotating frame. It has the form

$$L = T + U = \frac{1}{2}\dot{\boldsymbol{r}} \cdot \dot{\boldsymbol{r}} + \dot{\boldsymbol{r}} \cdot \tilde{\boldsymbol{\omega}} \cdot \boldsymbol{r} + \frac{1}{2}\omega^2(x^2 + y^2) + U(\boldsymbol{r}), \tag{2.1.9}$$

where the rotating frame subscript has been dropped for conciseness. We now wish to non-dimensionalize Equation 2.1.9 so that non-dimensional equations of motion can be determined. Let

$$R = |\boldsymbol{r_2} - \boldsymbol{r_1}| \quad \& \quad \frac{1}{N} = \sqrt{\frac{R^3}{G(m_1 + m_2)}} \tag{2.1.10}$$

be the length and time scales respectively such that $\boldsymbol{r}' = \frac{\boldsymbol{r}}{\boldsymbol{R}}$ and $\dot{\boldsymbol{r}}' = \frac{\dot{\boldsymbol{r}}}{\boldsymbol{R}N}$. Applying them to Equation 2.1.9 yields a non-dimensional Lagrangian of the form

$$L' = \frac{1}{2}\dot{\boldsymbol{r}}' \cdot \dot{\boldsymbol{r}}' + \dot{\boldsymbol{r}}' \cdot \tilde{\hat{\boldsymbol{z}}} \cdot \boldsymbol{r}' + V \tag{2.1.11}$$

where

$$V = \frac{1}{2}(x'^2 + y'^2) + \frac{1-\mu}{\sqrt{(x'+\mu)^2 + y'^2 + z'^2}} + \frac{\mu}{\sqrt{(x'-1+\mu)^2 + y'^2 + z'^2}} \quad \& \quad \mu = \frac{m_2}{m_1 + m_2}. \tag{2.1.12}$$

As follows from Lagrangian dynamics, the equations of motion can be found via

$$\frac{\partial}{\partial t}\left(\frac{\partial L'}{\partial \dot{\boldsymbol{r}}'}\right) = \frac{\partial L'}{\partial \boldsymbol{r}'}. \tag{2.1.13}$$

Plugging Equation 2.1.11 into Equation 2.1.13 yields the non-dimensional equations of motion in component form as

$$\ddot{x} - 2\dot{y} = \frac{\partial V}{\partial x}\,, \quad \ddot{y} + 2\dot{x} = \frac{\partial V}{\partial x}\,, \quad \ddot{z} = \frac{\partial V}{\partial x}\,, \tag{2.1.14}$$

where the apostrophes denoting non-dimensional quantities have been dropped and V follows from Equation 2.1.12. Equation 2.1.14 is the non-dimensional equation of motion in component form for the CR3BP (synodic frame). These are the dynamical equations that will be utilized for the remainder of this paper.

2.2 The CR3BP Jacobi Integral

An important property of the Lagrangian arises when it is not an explicit function of time. Recall that by assuming a circular orbit, we were able to remove the time dependence within the potential U. If we also look at the kinetic energy T in the rotating frame, we see a similar lack of dependence on time. As such when forming the Lagrangian, the only time-dependent quantities are the generalized coordinates $\boldsymbol{r}$ and $\dot{\boldsymbol{r}}$ which means that the Lagrangian is time-invariant. We will skip the specifics of the proof here, however, it can be shown that when L is time-invariant, there exists an integral of motion defined by

$$\frac{\partial L}{\partial \dot{\boldsymbol{q}}}\dot{\boldsymbol{q}} - L(\boldsymbol{q}, \dot{\boldsymbol{q}}) = const, \tag{2.2.1}$$

where $\boldsymbol{q}$ and $\dot{\boldsymbol{q}}$ represent the generalized coordinates of the system. This integral is called the Jacobi Integral. In the case of the non-dimensional CR3BP in the synodic frame, it follows as

$$J = \frac{1}{2}\dot{\boldsymbol{r}}\cdot\dot{\boldsymbol{r}} - \frac{1}{2}(x^2+y^2) - \frac{1-\mu}{\sqrt{(x+\mu)^2+y^2+z^2}} - \frac{\mu}{\sqrt{(x-1+\mu)^2+y^2+z^2}} = const. \tag{2.2.2}$$

2.3 Colinear Equilibrium Point Locations

In total, the CR3BP has five equilibrium (Lagrange) points denoted as L_i, $i = 1,2,3,4,5$. Of great importance are those that lie on the axis of primaries in the synodic frame. Given the names L_1, L_2, and L_3, families of periodic orbits (Lyapunov orbits) about these colinear points can be found by exploiting an inherent symmetry within the CR3BP. More on this will be discussed in a later section. For now, we will introduce the locations of the colinear Lagrange points for the non-dimensional system (see Fig. 1). The general procedure will be covered here, however, we recommend [4] for a more detailed derivation.

To determine the locations, we impose conditions on both the position and velocity components within the equations of motion. For the planar case, the state vector can be written as $\boldsymbol{X} = [x, y, \dot{x}, \dot{y}]^T$, which simplifies to $\boldsymbol{X}_{L_i} = [x_{L_i}, 0, 0, 0]^T$ when considering an equilibrium point on the axis of primaries. This allows for great simplification of the equations of motion wherein an equation in terms of x_{L_i} (the position of the equilibrium point) can be obtained. Imposing a change of variable and using the necessary intervals yields the following three quintic polynomials

$$\begin{aligned} L_1 \quad &: \quad \gamma_1^5 + (3-\mu)\gamma_1^4 + (3-2\mu)\gamma_1^3 + \mu\gamma_1^2 + 2\mu\gamma_1 + \mu = 0, \\ L_2 \quad &: \quad \gamma_2^5 + (3-\mu)\gamma_2^4 + (3-2\mu)\gamma_2^3 - \mu\gamma_2^2 - 2\mu\gamma_2 - \mu = 0, \\ L_3 \quad &: \quad \gamma_3^5 + (3-\mu)\gamma_3^4 + (3-2\mu)\gamma_3^3 + (2-\mu)\gamma_3^2 + 2\mu\gamma_3 + \mu = 0, \end{aligned} \tag{2.3.1}$$

where $\gamma_i = x_{L_i} - (1-\mu)$ represents the distance L_i is from the secondary body. Each polynomial will have one real root and four complex roots, the real root is the desired solution. This can then be used to find the location (x_{L_i}) of the colinear point.

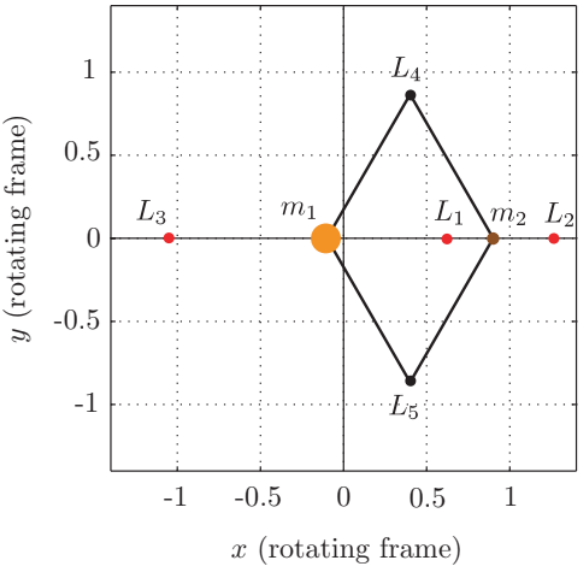

Fig. 1: Non-dimensional CR3BP Lagrange point locations for $\mu = 0.1$. [4]

3 Solution Techniques

3.1 Eigenvector Analysis of Dynamics about Colinear Lagrange Points

In order to determine the initial condition of a Lyapunov orbit, we must first find a suitable guess. To do so we analyze the solution to the linearized dynamics about the Lagrange point in question. The following explanation will be a high-level overview of the matter for points L_1 and L_2, however, a similar procedure can be carried out for L_3. Further, should a more detailed explanation be desired, one can similarly be found in [4]. We also note that for the remainder of this paper, we will consider the planar case of the CR3BP wherein motion is constrained to the x-y plane.

Linearizing Equation 2.1.14 about the colinear point x_{L_i} and inputting into matrix form yields

$$\begin{bmatrix} \dot{x} \\ \dot{y} \\ \dot{v}_x \\ \dot{v}_y \end{bmatrix} = \begin{bmatrix} 0 & 0 & 1 & 0 \\ 0 & 0 & 0 & 1 \\ a & 0 & 0 & 2 \\ 0 & -b & -2 & 0 \end{bmatrix} \begin{bmatrix} x \\ y \\ v_x \\ v_y \end{bmatrix}, \tag{3.1.1}$$

where

$$a = 2\bar{\mu} + 1 \quad , \quad b = \bar{\mu} - 1 \quad , \quad \& \quad \bar{\mu} = \frac{\mu}{|x_{L_i} - 1 + \mu|^3} + \frac{1-\mu}{|x_{L_i} + \mu|^3}. \tag{3.1.2}$$

Computation of the eigenvalues for the system above will show two purely real solutions ($\pm\lambda$) and two purely imaginary solutions ($\pm i\nu$). The existence of a positive real solution is enough to show that these points are unstable, however, the imaginary solution implies oscillatory motion (periodic orbits).

After some cumbersome algebra, it can be shown that the associated eigenvectors have the form

$$u_1 = \begin{bmatrix} 1 \\ -\sigma \\ \lambda \\ -\lambda\sigma \end{bmatrix} \quad , \quad u_2 = \begin{bmatrix} 1 \\ \sigma \\ -\lambda \\ -\lambda\sigma \end{bmatrix} \quad , \quad w = \begin{bmatrix} 1 \\ -i\tau \\ i\nu \\ \nu\tau \end{bmatrix} \quad , \quad \bar{w} = \begin{bmatrix} 1 \\ i\tau \\ -i\nu \\ \nu\tau \end{bmatrix}, \tag{3.1.3}$$

where u_1 and u_2 are eigenvectors for $\pm\lambda$ respectively, w and $\bar{w}$ are eigenvectors for $\pm i\nu$ respectively, and σ and τ are positive constants that can be found analytically. Noting that we are concerned with oscillating solutions and that the imaginary eigenvectors are complex conjugates, we need only analyze one of them. Splitting w into its real and imaginary components so that

$$w = \begin{bmatrix} 1 \\ 0 \\ 0 \\ \nu\tau \end{bmatrix} + i \begin{bmatrix} 0 \\ -\tau \\ \nu \\ 0 \end{bmatrix}, \tag{3.1.4}$$

it becomes easier to see how the dynamics are affected. Looking at the real vector, a displacement in x (1) and a change in $\dot{y}$ ($\nu\tau$) from the Lagrange point will provide a periodic solution. Conversely, looking at the imaginary vector, a displacement in y ($-\tau$) and change in the $\dot{x}$ (ν) from the Lagrange point will similarly provide the same solution.

Therefore, the formation of an initial guess is as simple as determining one of the imaginary eigenvectors associated with the linearized dynamics, separating its real and imaginary components, and then changing either set of components by a multiplier. For our purposes, we change only the real components such that the x displacement is positive and the change in $\dot{y}$ is negative. This yields a clockwise Lyapunov orbit starting from the positive-facing x-axis. The initial conditions will therefore have the form

$$\boldsymbol{X}_0 = \begin{bmatrix} x_{L_i} \\ 0 \\ 0 \\ 0 \end{bmatrix} + k \begin{bmatrix} 1 \\ 0 \\ 0 \\ -\nu\tau \end{bmatrix}, \tag{3.1.5}$$

where x_{L_i} is the colinear Lagrange point location and k is a displacement multiplier.

3.2 Differential Correction for Lyapunov Orbits

Now that an initial guess for the Lyapunov orbit has been determined, a method for iterating and refining the initial state can be employed. It is here we will return to the inherent symmetry within the CR3BP that can be exploited to simplify the computation. Specifically, there exists a mirrored trajectory on the opposite side of the axis of primaries for every initial condition lying on this axis. Therefore, if we choose an initial condition corresponding to a perpendicular trajectory ($\dot{x} = 0$), we can analyze the recrossing characteristics to determine the associated orbit's periodicity. Should this recrossing also be perpendicular, then the mirrored trajectories have formed a continuous closed curve and the orbit is periodic (see Fig. 2). Furthermore, this dependence on continuity allows for initial conditions to be refined until a propagated trajectory and its mirrored trajectory meet perpendicularly along the axis of primaries. This refinement process is known as differential correction.

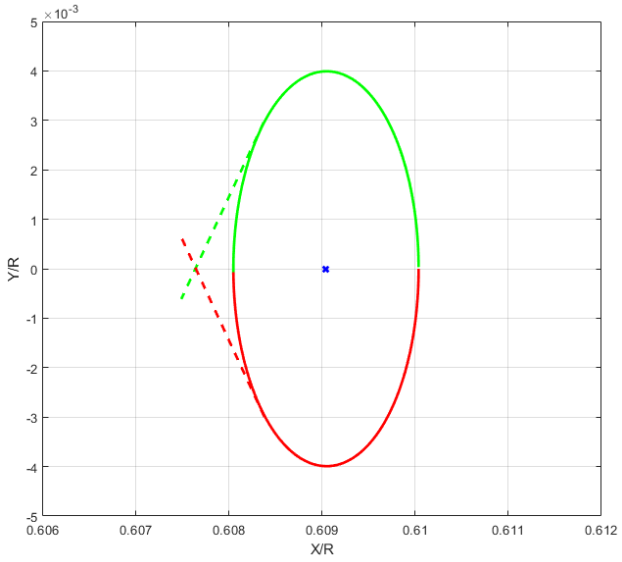

Fig. 2: Propagated trajectory (red) and mirrored trajectory (green) with their respective continuous (solid) and non-continuous (dashed) meeting points.

To accomplish this, we introduce the state transition matrix (STM, $\Phi(t, t_0)$) which is an n by n matrix that maps the state at an initial epoch t_0 to a state at another epoch t, that is

$$\boldsymbol{X}(t) = \Phi(t, t_0)\boldsymbol{X}(t_0). \tag{3.2.1}$$

For brevity, we will skip directly to the final result of the linearized system of equations relating the deviation in the final state to the deviation in the initial state. However, should a more in-depth analysis be desired, it can be found in [5].

Let $\boldsymbol{X}_k$ represent the state at t_k, $\partial\boldsymbol{X}_k$ represent the deviation in the state at t_k, and ∂T be the deviation in the orbit's period, then the linearized system of equations follows as

$$\partial\boldsymbol{X}_T = \Phi(T, t_0)\partial\boldsymbol{X}_0 + \frac{\partial\boldsymbol{X}_T}{\partial t}\partial T. \tag{3.2.2}$$

Before utilizing Equation 3.2.2, we must note an extra significance when analyzing perpendicular crossings. Let the subscripts 0 and $T/2$ represent states at the initial position and recrossing point (half the orbit's period) respectively. Now let the superscripts i and f represent, respectively, the states before and after the correction has been applied. Furthermore, let the deviation of an arbitrary state k be given by

$$\partial\boldsymbol{X}_k = \boldsymbol{X}_k^f - \boldsymbol{X}_k^i. \tag{3.2.3}$$

If we desire the initial state to lie at a particular point on the axis of primaries and be a perpendicular crossing, then the initial states before and after the correction will only differ by some deviation along the axis of primaries and some deviation in the y component of velocity, that is

$$\partial \boldsymbol{X}_0 = \begin{bmatrix} \partial x_0 \\ 0 \\ 0 \\ \partial \dot{y}_0 \end{bmatrix} = \boldsymbol{X}_0^f - \boldsymbol{X}_0^i = \begin{bmatrix} x_0^f \\ 0 \\ 0 \\ \dot{y}_0^f \end{bmatrix} - \begin{bmatrix} x_0^i \\ 0 \\ 0 \\ \dot{y}_0^i \end{bmatrix}. \tag{3.2.4}$$

If we then propagate the initial state before the correction forward, the state at the recrossing point will likely not be perpendicular. Therefore, it will have a state vector of the form $\boldsymbol{X}_{T/2}^i = [x_{T/2}^i, 0, \dot{x}_{T/2}^i, \partial \dot{y}_{T/2}^i]^T$. Conversely, propagation of the initial corrected state forward will yield a perpendicular recrossing. The deviation at the recrossing is therefore given by

$$\partial \boldsymbol{X}_{T/2} = \begin{bmatrix} \partial x_{T/2} \\ 0 \\ -\dot{x}_{T/2}^i \\ \partial \dot{y}_{T/2} \end{bmatrix} = \boldsymbol{X}_{T/2}^f - \boldsymbol{X}_{T/2}^i = \begin{bmatrix} x_{T/2}^f \\ 0 \\ 0 \\ \dot{y}_{T/2}^f \end{bmatrix} - \begin{bmatrix} x_{T/2}^i \\ 0 \\ \dot{x}_{T/2}^i \\ \dot{y}_{T/2}^i \end{bmatrix}. \tag{3.2.5}$$

Plugging in Equations 3.2.4 and 3.2.5 into Equation 3.2.2, the mapping becomes

$$\begin{bmatrix} \partial x_{T/2} \\ 0 \\ -\dot{x}_{T/2}^i \\ \partial \dot{y}_{T/2} \end{bmatrix} = \begin{bmatrix} \phi_{11} & \phi_{12} & \phi_{13} & \phi_{14} \\ \phi_{21} & \phi_{22} & \phi_{23} & \phi_{24} \\ \phi_{31} & \phi_{32} & \phi_{33} & \phi_{34} \\ \phi_{41} & \phi_{42} & \phi_{43} & \phi_{44} \end{bmatrix} \begin{bmatrix} \partial x_0 \\ 0 \\ 0 \\ \partial \dot{y}_0 \end{bmatrix} + \begin{bmatrix} \ddot{x}_{T/2}^i \\ \dot{y}_{T/2}^i \\ \ddot{x}_{T/2}^i \\ \ddot{y}_{T/2}^i \end{bmatrix} \partial(T/2). \tag{3.2.6}$$

The second row of Equation 3.2.6 can be used to solve for the deviation in the orbit period. It follows as

$$\partial(T/2) = \frac{-\phi_{21}\partial x_0 - \phi_{24}\partial \dot{y}_0}{\dot{y}_{T/2}^i}. \tag{3.2.7}$$

Plugging this result into row three of Equation 3.2.6 yields

$$-\dot{x}_{T/2}^i = (\phi_{31} - \frac{\ddot{x}_{T/2}^i}{\dot{y}_{T/2}^i}\phi_{21})\partial x_0 + (\phi_{34} - \frac{\ddot{x}_{T/2}^i}{\dot{y}_{T/2}^i}\phi_{24})\partial \dot{y}_0. \tag{3.2.8}$$

By further forcing the x component of position in the initial state to be constant, the deviation drops out, and solving Equation 3.2.8 for the deviation in the initial y component of velocity yields

$$\partial \dot{y}_0 = \frac{-\dot{x}_{T/2}^i}{(\phi_{34} - \frac{\ddot{x}_{T/2}^i}{\dot{y}_{T/2}^i}\phi_{24})}. \tag{3.2.9}$$

Although simple, Equation 3.2.9 is a powerful result. Here is an outline of its utility in refining the initial state.

1) Propagate the initial state guess and STM to just before the next x-axis crossing, roughly half the full Lyapunov period ($t = [0,\ T_L/2 - \partial t]$). Note that a good guess for a Lyapunov orbit's period is roughly half that of the primaries. Therefore, $T_L = \frac{1}{2}(2\pi)$.

2) Propagate the end state and STM from step 1 forward until the y component of the position is sufficiently close to zero. This indicates the state at the crossing has been found.

3) Use the state and STM at the crossing ($\boldsymbol{X}_{T/2}$, $\Phi(T/2,0)$) in conjunction with Equation 3.2.9 to determine the change in the initial y component of velocity required.

4) Update the initial state ($\boldsymbol{X}_0 = \boldsymbol{X}_0 + [0,0,0,\partial\dot{y}_0]^T$) and repeat steps until the magnitude of the x component of the velocity at the crossing is sufficiently close to zero. This implies the crossing is a perpendicular trajectory.

Once converged, this new initial state can be used to find the full Lyapunov orbit by integrating the equations of motion over the orbit's period. This period can be obtained from the last iteration of the above steps.

We must give a note of caution, the above method will hold only for small distances away from the colinear point. This is due to the linearized dynamics used in the derivation of Equation 3.2.9. If a sufficiently large k is chosen for use in Equation 3.1.5, the initial condition will no longer be within the linear envelope of the linearized dynamics. This will lead to an inability to find a Lyapunov orbit around the desired colinear lagrange point.

3.3 Manifold Trajectories to and from Lyapunov Orbits

To determine the full continuum of planar manifold trajectories to the propagated Lyapunov orbit, we employ eigenvector analysis of the monodromy matrix. Simply put, the monodromy matrix is the STM at the epoch corresponding to one full period of the Lyapunov orbit. If we then find the stable and unstable eigenvectors associated with this matrix, we can perturb points along the orbit in these directions. If this is done for a sufficient amount of points along the Lyapunov orbit, then a full continuum of planar manifold trajectories can be determined.

Let $\boldsymbol{V}_M$ be the stable or unstable eigenvector associated with the monodromy matrix and ϵ be a small number much less than one. The manifold trajectories associated with the current point on the Lyapunov orbit ($\boldsymbol{X}_i$) are therefore found by integrating the following deviated state,

$$\boldsymbol{X}_{manifold} = \boldsymbol{X}_i + \frac{\boldsymbol{V}_M}{|\boldsymbol{V}_M|}\epsilon. \tag{3.3.1}$$

If the stable eigenvector is used, then we must integrate backward in time. Conversely, if the unstable eigenvector is used, then we must integrate forward in time.

Integration of enough points along the orbit will lead to the formation of manifold tubes. These tubes allow a visual representation of the stable and unstable trajectory bounds to and from the orbit. It is within this context that we base the purpose of our paper.

4 Results

4.1 Periodic Orbits about L2

The following analysis focuses on a Lyapunov orbit about L2. Using the methods above, periodic orbits and their unstable and stable manifolds were plotted using MATLAB. This section focuses on a specific Lyapunov orbit that has an initial positive x displacement of 3840 kilometers (non-dimensional displacement of 0.0029) from the location of L2. The location of L2 of the Saturn-Titan system was determined using Equation 2.3.1 to be 1251908 km in the position x direction from the systems barycenter, corresponding to 52192 km in the positive x direction from the center of Titan.

Using the real part of the eigenvector that is associated with the complex eigenvalues of the linearized dynamics of L2 (as described in Section 3.1), a guess of the initial state that would propagate into a periodic orbit is found to be $\boldsymbol{X}_0 = \begin{bmatrix}1.04615 & 0 & 0 & -0.018207\end{bmatrix}'$. Propagating this initial state forward in time using

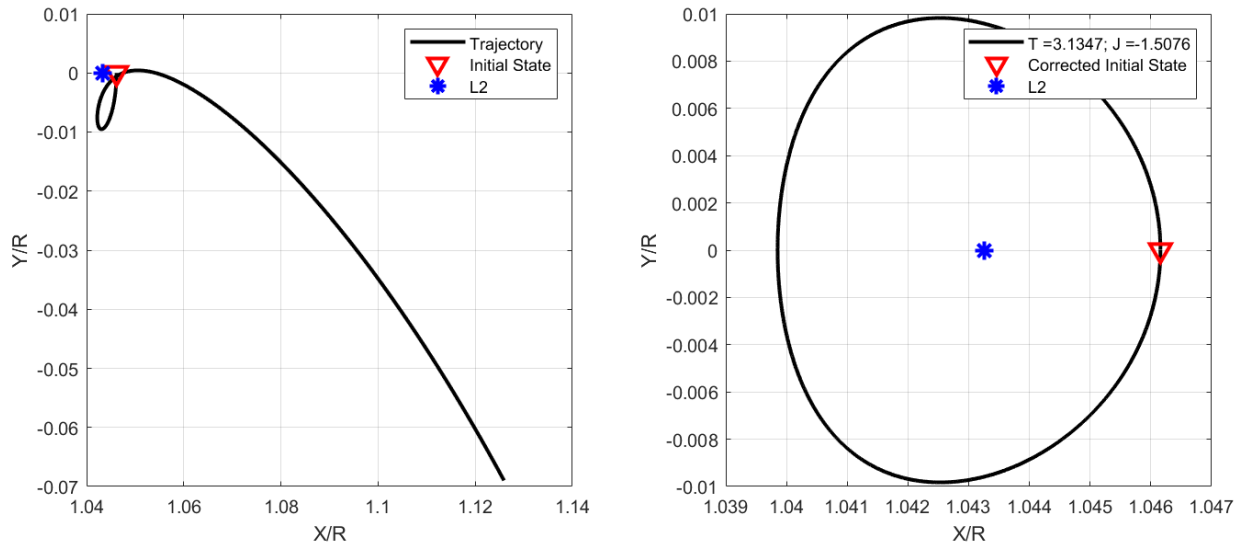

Fig. 3: Pre-corrected trajectory (left) and corrected trajectory (right)

the CR3BP dynamics formulated in Section 2.1 results in the trajectory shown in the left side of Figure 3, which quickly falls away from the Lagrange point.

Applying differential corrections to the initial guess using Equation 3.2.9 and the outline described at the end of Section 3.2 results in a corrected initial state of $\boldsymbol{X}_0, corrected = \begin{bmatrix} 1.04615 & 0 & 0 & -0.01934 \end{bmatrix}'$. Propagating this corrected initial state forward produces the periodic orbit about L2 shown in the right side of Figure 3. It is important to note that this method does not change the initial location of the guess, rather just manipulates the guessed initial velocity which remains perpendicular to the x-axis.

Using Equation 2.2.2, the non-dimensionalized Jacobi Integral for this orbit can be determined to be -1.5075. We can ensure our model is accurate by making sure this value stays constant over the entire integration period. Although not shown here, this value is shown to be constant in our model; see code.

4.2 Analysis of Periodic Orbit Stable and Unstable Manifolds

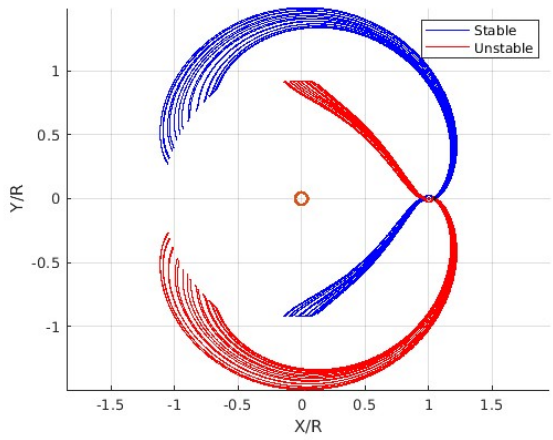

Fig. 4: Stable and Unstable Manifold Tubes of Lyapunov Orbit about L2

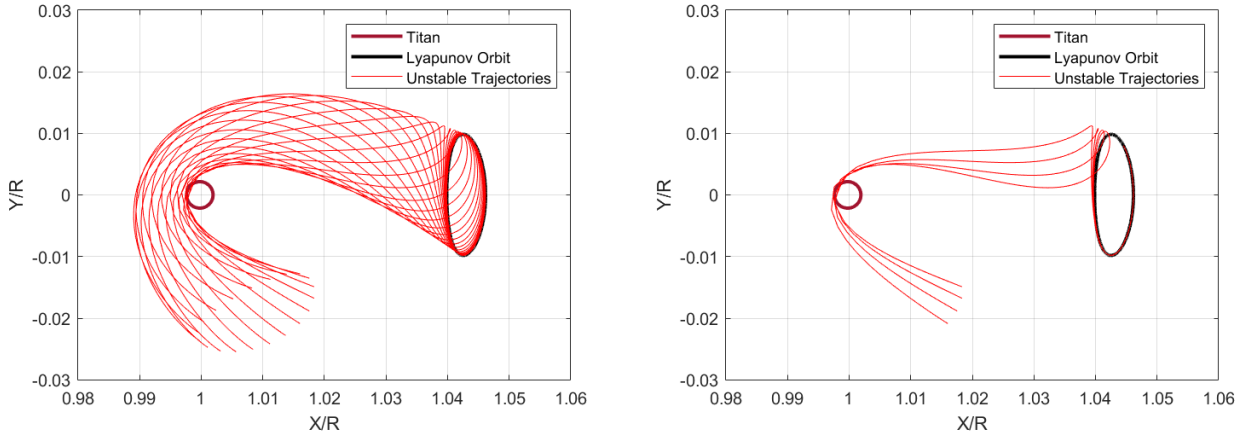

Fig. 5: Full unstable manifold looping around Titan (left) and those that intercept Titan (right)

Each point along the periodic orbit has its own corresponding stable and unstable manifolds in the direction of the respective stable and unstable eigenvectors of the orbit's monodromy matrix. To get a full understanding of the periodic orbits stable and unstable manifold, perturbations in the stable and unstable directions were propagated at 20 equally spaced points along the orbit, resulting in Figure 4. These 'tubes' provide a passage of transport for a non-propulsed satellite. Properly situating a satellite within these tubes will result in the satellite either moving away (unstable manifolds) or towards (stable manifolds) the periodic orbit.

To determine a fuel and time efficient descent trajectories into the atmosphere of Titan, the unstable manifold tube that develops towards Titan can be analyzed. The left side of Figure 5 shows each point's unstable manifold that develops into the tube that loops around the other side of Titan. While many of these trajectories will eventually intersect with Titan after a few more loops around the moon, this type of behavior is not desired as it increases the time and uncertainty of the maneuver.

Each trajectory was checked for an intersection of Titan and its atmosphere, resulting in the right side Figure 5. Analyzing the perturbed states of these manifolds provides a section of the orbit where a small perturbation in the right direction can result in a fuel and time efficient descent into the atmosphere of Titan.

5 Conclusions

By taking advantage of the dynamics of the Saturn-Titan system, a mission to land on the surface of Titan can be made both efficient and multi-faceted. This paper has shown that by accurately positioning a satellite on a stable manifold of certain Lyapunov Orbits about L2 while entering the system, a satellite can perform a fuel efficient transport onto a periodic orbit that provides great potential for examining Titan over a long period of time. Once this period of research ends, unstable manifolds can be used to quickly descend into the atmosphere of Titan and a landing exercise can be performed.

Further research will have to be done on the satellite maneuvers that would ensure the satellite reaches a stable manifold of a desired Lyapunov Orbit. Our model also lacks proper fidelity, and future models should include perturbations from the non-uniform gravitational fields of Saturn and Titan, distance gravitational bodies like the Sun, and atmospheric drag during the descent towards Titan.

The algorithm produced for this report is best utilized as a visual tool to examine the properties of Lyapunov orbits about the co-linear Lagrange points in any system where the eccentricity is close to zero. General fuel efficient missions can be formulated by analyzing specific manifold trajectories of the Lyapunov orbits that the algorithm determines.

6 Bibliography

[1] NASA. *Saturn's Moon Titan*, NASA Science, https://science.nasa.gov/saturn/moons/titan/. Accessed (2024)

[2] NASA. *Titan Exploration*, NASA Science, https://science.nasa.gov/saturn/moons/titan/exploration/. Accessed (2024)

[3] E.S. Gawlik, J.E. Marsden, S. Campagnola, A. Moore. *Invariant Manifolds, Discrete Mechanics, and Trajectory Design for a Mission to Titan*, (2009)

[4] W.S. Koon, M.W. Lo, J.E. Marsden, S.D. Ross, *Dynamical Systems, the Three-Body Problem and Space Mission Design*, (2022)

[5] B.D. Tapley, B.E. Schutz, G.H. Born, *Statistical Orbit Determination*, (2004).

[6] Rosengren, Aaron J., MAE 240 S24, *Newtonian Formulation*, *Lagrangian Formulation*, *Hamiltonian Formulation*, *Numerical Methods*. University of California San Diego, Department of Mechanical and Aerospace Engineering.

[7] H. Pollard, *Mathematical Introduction to Celestial Mechanics*, (1966).

[8] D.J. Scheeres, *Orbital Motion in Strongly Perturbed Environments*, (2012).